LANGMUIR

pubs.acs.org/Langmuir Article

Structural Effects of Cation Binding to DPPC Monolayers

Matti Javanainen,* Wei Hua, Ondrej Tichacek, Pauline Delcroix, Lukasz Cwiklik, and Heather C. Allen*



Cite This: Langmuir 2020, 36, 15258-15269



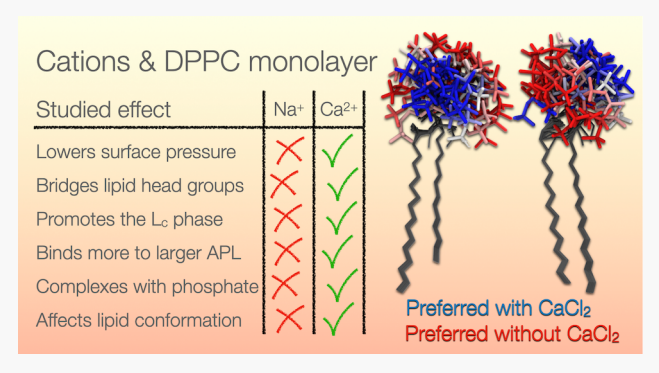
ACCESS

III Metrics & More



SI Supporting Information

ABSTRACT: Ions at the two sides of the plasma membrane maintain the transmembrane potential, participate in signaling, and affect the properties of the membrane itself. The extracellular leaflet is particularly enriched in phosphatidylcholine lipids and under the influence of Na⁺, Ca²⁺, and Cl⁻ ions. In this work, we combined molecular dynamics simulations performed using state-of-the-art models with vibrational sum frequency generation (VSFG) spectroscopy to study the effects of these key ions on the structure of dipalmitoylphosphatidylcholine. We used lipid monolayers as a proxy for membranes, as this approach enabled a direct comparison between simulation and experiment. We find that the effects of Na⁺ are minor. Ca²⁺, on the other hand, strongly affects the lipid headgroup conformations and induces a tighter packing of lipids,



thus promoting the liquid condensed phase. It does so by binding to both the phosphate and carbonyl oxygens via direct and water-mediated binding modes, the ratios of which depend on the monolayer packing. Clustering analysis performed on simulation data revealed that changes in area per lipid or CaCl₂ concentration both affect the headgroup conformations, yet their effects are anticorrelated. Cations at the monolayer surface also attract Cl⁻, which at large CaCl₂ concentrations penetrates deep to the monolayer. This phenomenon coincides with a radical change in the VSFG spectra of the phosphate group, thus indicating the emergence of a new binding mode.

■ INTRODUCTION

Concentration gradients of cations across cellular membranes are required to maintain the electrostatic potentials across these membranes. This potential can be harnessed to drive transmembrane processes, and its localized changes are used as a means of signaling. Moreover, cations such as calcium also directly participate in numerous signaling pathways at the membrane surface. 1-3 Cation adsorption can also affect the lateral structure of lipid membranes and vice versa, 4-6 which could regulate membrane protein function via membranemediated effects. Therefore, understanding the interactions between cations and lipid membranes is of crucial interest, a task best tackled with a collaboration between simulations and experiments. Indeed, numerous molecular dynamics (MD) simulation studies have focused on lipid-ion interactions in an attempt to reveal atom-level information on these interactions. 6-10 Unfortunately, it has only recently become evident that in most of these studies the adsorption of both sodium and calcium onto phosphatidylcholine (PC) head groups has been significantly overestimated.⁸ Indeed, different approaches based on either charge scaling or additional repulsive potentials have been recently introduced to tackle this problem. 11-14 This issue and the underlying reasons related to the lack of polarization effects in common classical force fields are discussed in our recent review.14

While lipid bilayer simulations are routinely performed in silico, they are often not convenient to study experimentally. Therefore, lipid monolayers are often used as a model of the bilayer. In contrast, MD simulations have traditionally struggled with lipid monolayers due to the inadequate description of water—air interfaces. These compatibility issues between experiment and simulation have traditionally prevented quantitative and interdisciplinary studies on lipid—ion interactions.

In this work, to overcome the aforementioned issues, we complemented experimental work on lipid monolayers with simulations that bring together three key methodological improvements in the field. Namely, we combined a recent ECC lipid model by Melcr et al., ¹¹ the ECC ions, ^{17–19} and the optimal point charge (OPC) water model. The ECC ("electronic continuum correction") ions account for electronic polarizability in a mean-field manner by using scaled-down charges. The ECC lipid model is based on the Lipid14²⁰ model and describes the adsorption of ECC ions onto the PC

Received: August 28, 2020 Revised: November 24, 2020 Published: December 9, 2020





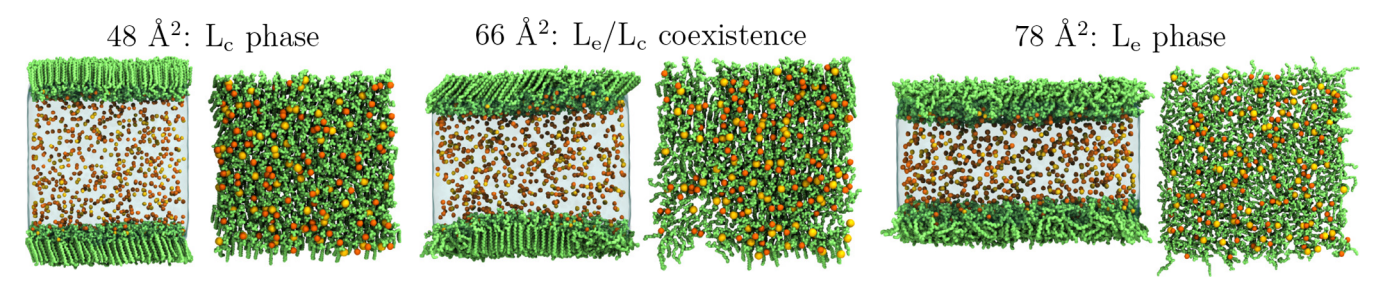


Figure 1. Side and top views of selected systems with 410 mM CaCl₂ and at varying APLs. These correspond to the L_c phase (48 Å²), the L_e phase (78 Å²), and their coexistence (66 Å²). DPPC is shown in green, Ca²⁺ in yellow, Cl⁻ in orange, and water as a transparent blue surface. Hydrogens are omitted for clarity. All simulation boxes span 22 nm in the direction normal to the monolayer plane, yet this vacuum space is also omitted in the representation.

headgroup region with a significantly larger accuracy than any other commonly used combination of lipid and ion models.^{8,11} Finally, the OPC water model²¹ was recently shown to be able to describe lipid monolayer behavior,^{22,23} and thus avoid many of the issues with MD simulations of such systems.¹⁶

With this state-of-the-art set of force fields and in combination with Langmuir trough measurements and vibrational sum frequency generation (VSFG) spectroscopy, we studied the effect of the key cations—Na⁺ and Ca²⁺—on the properties of DPPC monolayers. While such monolayes serve as models for lipid membranes, they are also interesting in the context of the DPPC-rich pulmonary surfactant. ^{24,25}

We found that Na⁺ has little effect on the monolayer properties. However, Ca²⁺ causes a significant decrease in the surface pressure of the monolayer by favoring the presence of the liquid condensed phase, which in a constant area ensemble leads to looser packing of the liquid expanded phase. We also found that a few hundred millimolar concentrations of CaCl₂ are able to induce this effect, whereas larger concentrations do not have a substantial effect on the surface pressure. Nevertheless, at these larger concentrations, lipid headgroup conformations are still affected as both Ca²⁺ and Cl⁻ are able to penetrate and bind deep into the lipid carbonyl region and displace hydration water. This observation is supported by the VSFG spectra of phosphate stretching, which also indicates an emergence of a specific Ca²⁺-PO₄²⁻ complex.

METHODS

Simulation Models and Methods. Atomistic classical molecular dynamics simulations were performed to unravel the effect of cations on the structure of a dipalmitoylphosphatidylcholine (DPPC) monolayer. The simulated systems contained 512 DPPC molecules in two independent monolayers, each with 256 lipids. These lipid films were located at the water-air (or technically water-vacuum) interfaces formed on a slab of ~40 000 water molecules located in the middle of a periodic simulation box. Monolayers with eight area per lipid (APL) values (42, 48, 54, 60, 66, 72, 78, 90 Å²) were simulated. Hence, the simulated systems captured the liquid condensed (L_c) and liquid expanded (L_e) phases as well as their coexistence. The lateral sizes of the simulation box ranged from approximately $10 \times 10 \text{ nm}^2$ to $15 \times 15 \text{ nm}^2$. The box was elongated to 22 nm in the direction normal to the interface in order to avoid long-range electrostatic interactions of lipids through the vacuum (air) phase. Snapshots of the monolayer at three different APL values are shown in Figure 1.

In terms of solvent, either pure water or solutions of NaCl or CaCl₂ were considered. For NaCl, 600 Na⁺ and Cl⁻ ions were inserted, which yielded a concentration of 820 mM. For CaCl₂, 300 Ca²⁺ ions were included with twice the amount of Cl⁻ counterions to provide a concentration of 410 mM. Additionally, monolayers with APLs equal to 48, 66, and 78 Å², corresponding to the L_c phase, L_c/L_e coexistence, and the L_e phase, were simulated with different amounts of CaCl₂. To

this end, 75, 150, 300, 750, or 1500 Ca²⁺ ions were included with twice the amount of Cl⁻ counterions to provide concentrations of 101 mM, 203 mM, 1.06 M, and 2.25 M (note that ions are added by replacing water molecules with them). These CaCl₂ concentrations are significantly larger than those present in cellular environments. However, the values reported above are total concentrations, and adsorption to lipid head groups will decrease the concentration of freecations in the solution. Especially in cellular environments with charged lipids, this effect could be significant. In addition, the ocean and marine atmospheric aerosol—particularly aerosol that become dehydrated during transport over arid continental regions—contain relatively high concentrations of ions, notably, Cl⁻, Na⁺, Mg²⁺, Ca²⁺, SO₄²⁻, and K^{+,26} A practical reason for using such high concentrations is that the isotherms in a Langmuir trough are not substantially altered with some ions, and therefore the observed effects are amplified by exaggerating the salt concentrations. A similar issue also haunts simulations, where a physiologically relevant CaCl₂ concentration would correspond to few ions in the simulation box.

In the case of both pure water and NaCl, 200 ns-long trajectories were simulated whereas 300 ns-long trajectories were collected for the systems containing CaCl₂. Notably, the time scale in which equilibrium of ion adsorption/desorption is achieved is significantly shorter with ECC ions that with full charge ones.^{8,11} In each case, the last 100 ns were used for analyses. Simulations were performed employing canonical (NVT) ensemble at a temperature of 298 K. The canonical ensemble is commonly used for monolayer simulations, and it was chosen here over the constant-tension ensemble to obtain surface pressure—area isotherms in which the molecular area on the abscissa is uniformly spaced. The simulation outputs are available at doi.org/10.5281/zenodo.1043958 (no ions), doi.org/10.5281/zenodo.1043956 (NaCl), and doi.org/10.5281/zenodo.1154569 (CaCl.).

To accurately capture both the lipid behavior at a water-air interface and the cation affinity for the PC headgroup, we combined a set of state-of-the-art force fields. Lipids were modeled using the headgroup parameters adapted from ECC-POPC, 11 which is based on Lipid14. 20 This lipid model was parametrized to capture the headgroup responses to cations when combined with the ion models developed by the group of Prof. Pavel Jungwirth. 17-19 Briefly, these ion models account for electronic polarizability in a mean field manner by adapting the electronic continuum correlation (ECC) approach. 12,14,27,28 Effectively, the charges of the ions are scaled by a factor of 0.75 and the Lennard-Jones σ parameter is fine-tuned to agree with neutron scattering data. This cures the excessive adsorption of ions to zwitterionic lipid membranes present in many atomistic simulation models.⁸ Notably, the ECC approach allows for ionbridged lipid-protein binding, which presents a challenge for the NBFIX approach¹³ that relies on additional repulsive potentials between ions and positively charged lipid and protein groups.¹⁴ Finally, the OPC water model²¹ was recently demonstrated by us to provide a good agreement with experimental isotherms of lipid monolayers \$22,23 and was hence adapted to this work. Notably, the improvement over the commonly used TIP3P water model is significant. Since the ECC ions were parametrized with another water

model (SPC/E), we refined their σ parameters so that the first peak in the water—ion radial distribution function agreed with experimental findings (see Table S1 in the Supporting Information (SI)). We chose this metric for the fine-tuning, since the original ECC ion models were also based mainly on structural data. ^{17–19} Still, we only needed to adjust the σ of Na⁺ by a mere 0.02 nm, whereas no changes were required for either Ca²⁺ or Cl⁻. This indicates that the ECC parametrization is robust with respect to the used water model.

The simulations were performed using GROMACS v5.1.4.²⁹ Periodic boundary conditions were used in all directions and the Newtonian equations of motion were integrated with a time step of 2 fs. Lennard-Jones potential was shifted to zero at 1.2 nm, and the smooth particle mesh Ewald method³⁰ was used to calculate the long-range contribution to electrostatic interactions. The dispersion correction³¹ was applied to energy and pressure to account for long-range Lennard-Jones interactions. Neighbor lists were maintained using buffered Verlet lists.³² The temperatures of the lipids and the solvent were separately coupled to a stochastic velocity rescaling thermostat³³ with a target temperature of 298 K and a time constant of 1 ps. The bonds involving hydrogens were constrained using the LINCS algorithm.^{34,35}

Simulation Analyses. The surface pressures Π at an APL of A were calculated from the surface tensions γ measured from simulations as

$$\Pi(A) = \gamma_0 - \gamma(A) \tag{1}$$

where γ_0 is the surface tension of the lipid-free solvent—air interface, and due to the symmetry of the simulation system, γ is calculated simply as

$$\gamma = \frac{(P_{\rm N} - P_{\rm L}) \times L_z}{2} \tag{2}$$

where $P_{\rm N}$ and $P_{\rm L}=1/2\times(P_{xx}+P_{yy})$ are the normal and lateral components of the pressure, $P_{xx}=P_{yy}$ are the lateral components of the pressure tensor, and L_z is the length of the simulation box normal to the interface. The value of γ_0 is sensitive to ions so its values were extracted for all used ionic conditions from simulations without lipids.

The fractions of the L_e phase were calculated as in our previous work.²² The oxygen-cation contacts were measured with a cutoff of 0.325 nm as in our earlier work.6 This corresponds to the first minimum in the lipid oxygen-cation RDF, and the number of detected contacts is constant over a large range of cutoff values around the chosen one (see Figure S3 in ref 6). For chloride, we set the cutoff to 0.535 nm as it includes the first peak in the lipid oxygenchloride RDF. In the case of chloride, this first peak is not as welldefined as in the case of the cations, which leads to some level of arbitrariness in the calculated numbers of bound chlorides. Density profiles were calculated with the gmx density tool bundled with GROMACS. The profiles were centered based on the lipid coordinates, and symmetrized. The numbers of Ca²⁺ and Cl⁻ ions that penetrated beneath the phosphate region toward the carbonyl groups was calculated as follows: The number densities of the ions were integrated from the maximum of the phosphate density until the vacuum phase. This maximum density was obtained as the midpoint of a Gaussian fit to the phosphate density profile.

The relative numbers of ions bound directly and in a water-mediated manner (interaction bridged by a water due to its dipole moment) to lipids were calculated as follows: non-normalized radial distribution functions (RDFs) of ions around carbonyl and phosphorus (the two bound only to phosphorus) oxygens were calculated. The first peak (direct binding) was numerically integrated from 0 to 0.32 nm, which lies in the first wide minimum. For carbonyl, the top of the second peak was fitted with a Gaussian function and analytically integrated, whereas for phosphate a double Gaussian was used to capture the clearly visible bimodal distribution. These Gaussians were used as the RDF did not return to zero after the second peak and hence we wanted to avoid setting an arbitrary cutoff distance. The coordination numbers were estimated by integrating

RDFs of carbonyl and phosphate (the two bound only to phosphorus) oxygens up to the minimum after the second peak.

Conformations of the lipids were analyzed statistically by a computer clustering method. The clustering procedure automatically separates the population of lipids into several disjoint sets ("clusters") of lipids with a similar conformation and discover within each set a member that represents it in an average fashion, also called a "centroid". Consequent analysis can then be performed on a much smaller number of lipids (the centroids) and take into account the abundances of the sets to be used, for example, as weights.

Data from all simulations were combined and the pairwise interlipid distances were calculated. The distance was defined as the Euclidean distance between the positions of the headgroup atoms which were first aligned. The alignment (translation and rotation) was done in a pairwise fashion using a rigid part of glycerol backbone, namely the C1, C2, and C3 atoms. Hierarchical clustering method using the Ward's linkage method was applied on a total of 359 424 lipid conformations randomly sampled from 18 individual simulations with varying conditions (area per lipid of 48, 66, or 78 Å² and CaCl₂ concentration of 0, 101, 203, 410, 1060, or 2250 mM). The trajectory was preprocessed with the help of the MDAnalysis python package. The pairwise distance was calculated using an in-house developed software employing an optimized singular value decomposition method based on ref 37. and implemented by Eric V. Jang (https://github.com/ericjang/svd3). The clustering was carried out using a modified version of the scipy.cluster.hierarchy Python package https://github.com/scipy/scipy/tree/v1.5.2/scipy/cluster.

Deuterium order parameter for a carbon—hydrogen bond (or often carbon—deuterium bond in an experiment) is defined as $S_{\rm CD}=\frac{1}{2}$ $(3\cos^2\theta-1)$, where θ is the angle of the bond with respect to the normal of the membrane. Since the deuterium order parameter is a common way to characterize lipid chain ordering and headgroup conformations in lipid bilayers, 38 we decided to extract it from our simulations although the experiment is not feasible on monolayers. The $S_{\rm CD}$ values for the headgroup β and α carbons (see Figure 10) were calculated from the carbon and hydrogen positions with an inhouse script. The values for the two hydrogens were calculated and the mean and difference of these two values were reported as the value and its error estimate for each studied carbon.

Visualization was performed using the VMD Molecular Graphics Viewer³⁹ and rendered with the use of the Tachyon Ray Tracing System.⁴⁰

Materials. Sodium chloride (NaCl) (certified ACS, 99.5–100.5%) and calcium chloride hexahydrate (CaCl2·6H2O) (certified ACS, 99%) were purchased from Fisher Scientific (Waltham, MA). 1,2dipalmitoyl-sn-glycero-3-phosphocholine (DPPC) (>99%, Avanti Polar Lipids, Alabaster, AL) was used as received and dissolved in chloroform (>99.9%, HPLC grade, Sigma-Aldrich, St. Louis, MO) at a 1 mM concentration. Ultrapure water with a resistivity of 18.2-18.3 $M\Omega$ ·cm and measured pH of 5.6 (the pH is slightly acidic due to the dissolution of gaseous CO2) was obtained from a Barnstead Nanopure system (D4741, Thermolyne Corporation, Dubuque, IA) equipped with additional organic removing cartridges (D5026 Type I ORGANICfree Cartridge Kit; Pretreat Feed). Stock chloride salt solutions were prepared by dissolving salts in ultrapure water and pretreated according to procedures described previously to remove potential remaining organic contamination. 41 Concentrations of these solutions were standardized by Mohr titration.⁴² Once the concentrations were known, each salt stock solution was diluted to the desired concentrations. The measured pH of the salt solutions laid in the range 5-7. All salt solutions were shown to be free of organic impurities, as revealed by their VSFG spectra obtained in the surfactant CH stretching region (2800-3000 cm⁻¹). All solutions were thermally equilibrated to room temperature (23 \pm 1 °C) over 24 h prior to measurement.

VSFG Spectroscopy Measurements. VSFG spectra $(|\chi_S^{(2)}(\omega_{IR})|^2)$ from the lipid-covered aqueous surfaces were obtained on a broad-bandwidth VSFG spectrometer setup that has been described elsewhere.⁴³ The average visible/infrared (IR) pulse energy

of the visible (0.8 μ m) and IR (2.6-3.3 μ m and 8.3-10.0 μ m in the water OH and phosphate stretching regions, respectively) beams incident on the aqueous surface were 300/6 and 300/10 μ J for the phosphate and water OH spectral regions, respectively. Spectra were recorded with a 5 min integration time. All VSFG spectra were background-subtracted and normalized against the nonresonant VSFG spectrum from a GaAs(110) crystal (Lambda Research Optics, Costa Mesa, CA) to eliminate the spectral distortion caused by the frequency-dependent IR beam energy in the spectral region of interest. For each experiment, ultrapure water was poured (28 mL) in acid-cleaned Petri dishes (5 cm diameter) and spectra of the neat air/ water interface were used as a reference to assess reproducibility during the entire experimental period. Then, water was replaced by aqueous salt solutions onto which DPPC monolayers were overspread $(\sim 12 \mu L)$. Under this condition, DPPC monolayers were equilibrated in the highly ordered L_c phase as tested by surface tension measurement. The APL for DPPC molecule on neat water is approximately 41 Å². Prior to any spectroscopic measurements, 10 min was allowed for solvent evaporation. The ssp (s for sumfrequency, s for visible, and p for infrared) polarization combination was selected for all spectra presented here. All measurements were repeated at least three times to ensure reproducibility and were recorded at room temperature (23 ± 1 °C). Only every second data points are plotted in the VSFG spectra to avoid spectral clutter.

RESULTS

Ca2+ but Not Na+ Induces a Shift In the Pressure-**Area Isotherm.** We first calculated the surface pressure—area isotherms for DPPC in the presence and absence of ions and compared them against experimentally measured isotherms for similar systems.⁴⁴ In simulations, the surface tension of the pure water-air interface was calculated to be $70.9 \pm 0.3 \text{ mN/}$ m, in good agreement with the experimental value of 71.97 mN/m. The ions had little effect on this tension, yet the γ_0 value in eq 1 was still calculated separately for each ion concentration. As the surface tension values of electrolyte solutions used in this work in SI Figure S1 demonstrate, the used ECC ions^{17–19} underestimate the effect of increasing salt concentration (for a more complete plot, see our recent review¹⁴). This results from the fact that the charges should in principle be scaled by different factors at the two sides of the interface, which is also manifested by the fact that full charges tend to overestimate the dependence of surface tension on salt concentration. 14

Both experimental and computational isotherms are shown in Figure 2. The computational ones were calculated from the last 100 ns of simulation data so that the number of bound ions at the surface had equilibrated (see top row of SI Figure S2). The experimental isotherms (top panel, adapted from ref 44) show that NaCl has little effect on the shape and position of the isotherm, whereas CaCl₂ shifts the isotherm downward in the coexistence region. This behavior is also captured well in the computational isotherms (middle panel), where NaCl has little effect on the isotherms and CaCl2 mainly affects the pressure at the coexistence plateau. The numbers of cationlipid interactions, plotted in the bottom panel of Figure 2, reveal that Na+ binds little to the lipids regardless of the monolayer APL. Ca²⁺, on the other hand, binds much more to lipids, and the amount of bound cations depends on the APL. Between 42 and 60 Å², the cation-lipid contacts increase by ~40%. Further increase in APL does not increase the number of these contacts.

We also studied the interaction of the chloride ions with the lipids. A longer cutoff was used to analyze the lipid—ion contacts (see Methods) since Cl⁻ ions do not bind to the lipids

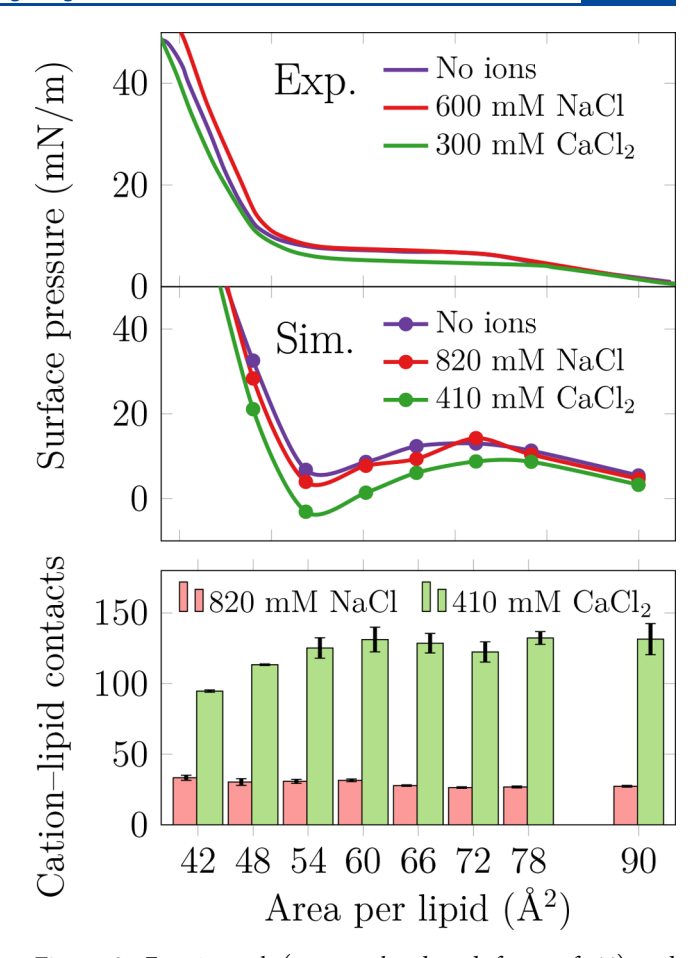


Figure 2. Experimental (top panel, adapted from ref 44) and simulated (middle panel) isotherms of the DPPC monolayer under various solvent environments. Note that the used concentrations between experiments and simulations are not equal. Still, in both cases NaCl has no effect on the isotherm, whereas CaCl₂ induces a downward shift especially in the $L_{\rm c}/L_{\rm e}$ coexistence region. The number of cation—lipid contacts is shown in the bottom panel, and the error bars show standard error obtained via block averaging. For NaCl, this number seems small and fairly independent of APL, although it is actually decreased by ~18% from smallest to largest area. For CaCl₂ the number of contacts increases by a total of 39% upon increasing APL, although the values seem to saturate at an APL of ~60 Ų.

directly, but instead are bridged to negative lipid groups via cations. As demonstrated in the bottom row in SI Figure S2, we observed that in the case of NaCl, the larger the APL, the more chlorides were located in the vicinity of the lipids. This is somewhat surprising considering that the number of bound Na⁺ ions is constant across the studied APLs. For CaCl₂, the Cl⁻ binding over time follows a similar pattern as that of Ca²⁺, and a similar dependency on APL is observed.

Ca²⁺ Bridges Lipid Head Groups and Thereby Promotes the L_c Phase. We next studied how the ions affect the packing of lipids at a nanoscopic level within the coexistence region. To this end, we calculated the fraction of lipid chains that were loosely packed and hence in the liquid expanded (L_e) phase. The analysis was adopted from our previous work, ²² and the results are shown in Figure 3. At 54 Å², the entire monolayer is in the liquid condensed (L_c) phase, whereas the fraction of the L_e phase grows steadily for lipid areas between 60 and 72 Å². Similar increase is observed

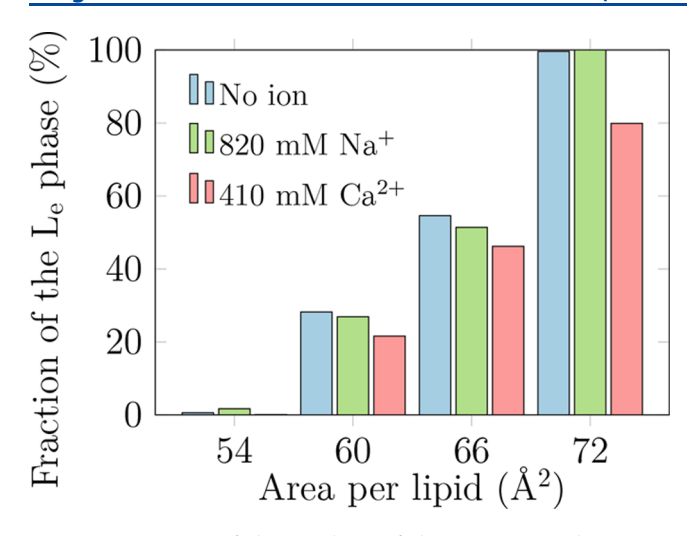


Figure 3. Fraction of the $L_{\rm e}$ phase of the DPPC monolayer as a function of solvent environment in systems that are within the $L_{\rm c}/L_{\rm e}$ coexistence plateau.

independently on the presence of ions, yet the values for the system with CaCl₂ are always somewhat lower than for the ion-free monolayer and the monolayer with NaCl. This indicates that CaCl₂ can induce tighter packing of the lipids, likely by clustering the head groups of multiple lipid molecules.

A detailed look into the direct binding modes of Ca^{2+} to lipid oxygens is provided in SI Figure S3. In the radial distribution functions (RDFs), this direct binding has a sharp distribution at 0.21-0.23 nm (see SI Figure S4). Upon growing area, the repulsion between cations decreases and thus more Ca^{2+} binds to the phosphate groups. In the carbonyl region the situation is different as the number of Ca^{2+} penetrating there is also much smaller. At the smallest area, less Ca^{2+} reaches the carbonyl region likely due to the compact packing, yet at larger areas the number of Ca^{2+} bound to carbonyls is fairly constant. Only at the largest area per lipid, the number of bound Ca^{2+} slightly decreases, likely due to the dynamic nature of the L_e phase monolayer which makes it difficult for the cations to engage in optimally coordinated binding modes.

In addition to these direct binding modes, we also analyzed the solvent-shared Ca^{2+} -lipid binding (see SI Figure S4 for a visualization). For carbonyl oxygens, the number of Ca^{2+} s bound via water molecules was \sim 2.2 times that of the directly bound ones and the former manifested itself in the RDFs as a single Gaussian peak centered at \sim 0.46 nm.

For the phosphates, the situation is quite different: The solvent-shared binding displayed a bimodal distribution with characteristic Ca²⁺—oxygen distances of 0.39 and 0.44 nm. These correspond to modes where the binding is coordinated by two or one water molecules, respectively. For the former, the Ca²⁺, oxygen, and the two waters form a rhombus-like shape and thus the Ca²⁺—oxygen distance is shorter than in the case of a single water bridging the Ca²⁺ and oxygen in a linear arrangement (see SI Figure S4). The conformation with a single shared water molecule was always more prevalent by ~50%. However, unlike for the carbonyls where the solvate-shared binding dominates, the number of Ca²⁺ bound by solvent-sharing to phosphate oxygens was 10% lower than the number of directly bound Ca²⁺.

The coordination number of carbonyl and phosphate oxygens around Ca²⁺ at 0.32 nm ranged from 1.0 to 1.4,

growing monotonously with area per lipid. However, a molecule can reside close to both carbonyl and phosphate oxygen of the same lipid, so our numbers are likely somewhat overestimated. At the end of the second peak in the Ca²⁺ – oxygen RDF at 0.53 nm, the coordination numbers ranged from 2.2 to 2.9. These numbers indicate that Ca²⁺ directly binds to one lipid, yet it can bind to another 1–2 lipids via solvent-shared binding.

Higher CaCl₂ Concentrations Affect Lipid Head Group Conformation Instead of Lipid Packing. Next, we studied the effect of $CaCl_2$ concentration on the monolayer at selected values for the area per lipid. These systems corresponded to the $L_{\rm e}$ and $L_{\rm c}$ phases as well their coexistence, and the studied total $CaCl_2$ concentrations were 101, 203, 410, 820, 1060, and 2250 mM. We again verified that the number of bound ions had stabilized before the last 100 ns of the simulation trajectory that was used in the analyses (see top row in SI Figure S5). It is also worth noting that since some cations adsorb to the lipid headgroup region, the concentrations of free Ca^{2+} in the aqueous phase can be significantly smaller than the total concentration, as demonstrated in SI Figure S6.

We first calculated the dependency of the surface pressure on the CaCl₂ concentration, which is shown in Figure 4. It is

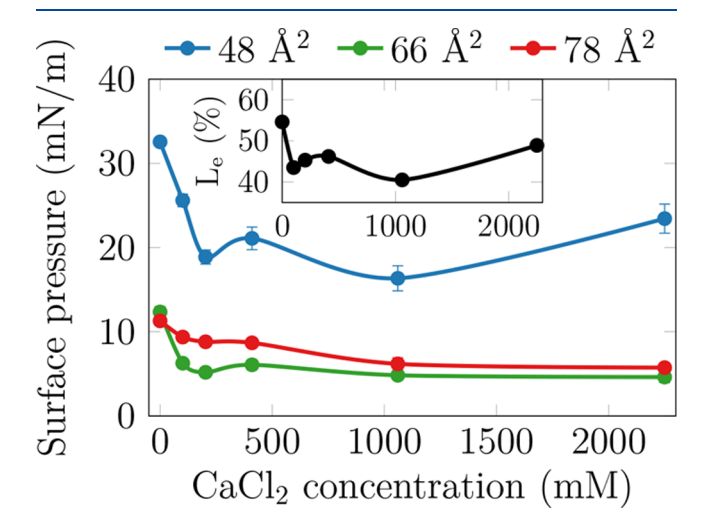


Figure 4. Surface pressures of the simulated DPPC monolayers in different phases as a function of $CaCl_2$ concentration. The inset shows the fraction of the L_e phase as a function of $CaCl_2$ concentration for the monolayer with an APL of 66 Å².

clear that at small $CaCl_2$ concentrations, the surface pressure values drops, yet the curves stabilize at around 400 mM. This could either mean that the monolayer is saturated with ions at that concentration, or that the additional adsorption of ions has no effect on the packing of the monolayer. Further analysis demonstrates that the effect of $CaCl_2$ concentration on the L_e fraction was also negligible at concentrations larger than 400 mM (see the inset of Figure 4.

The number of contacts between lipid oxygens and calcium ions, shown in Figure 5, reveal that no such saturation of ion adsorption is observed in the studied concentration range. This is also highlighted by the time evolution of the lipid—Ca²⁺ contacts shown on the top row of SI Figure S5. At small CaCl₂ concentrations, the binding to monolayers with different APLs and hence different phases is fairly equal, whereas at higher concentrations the adsorption to monolayers with larger APL values is substantially larger. At high CaCl₂ concentrations, the

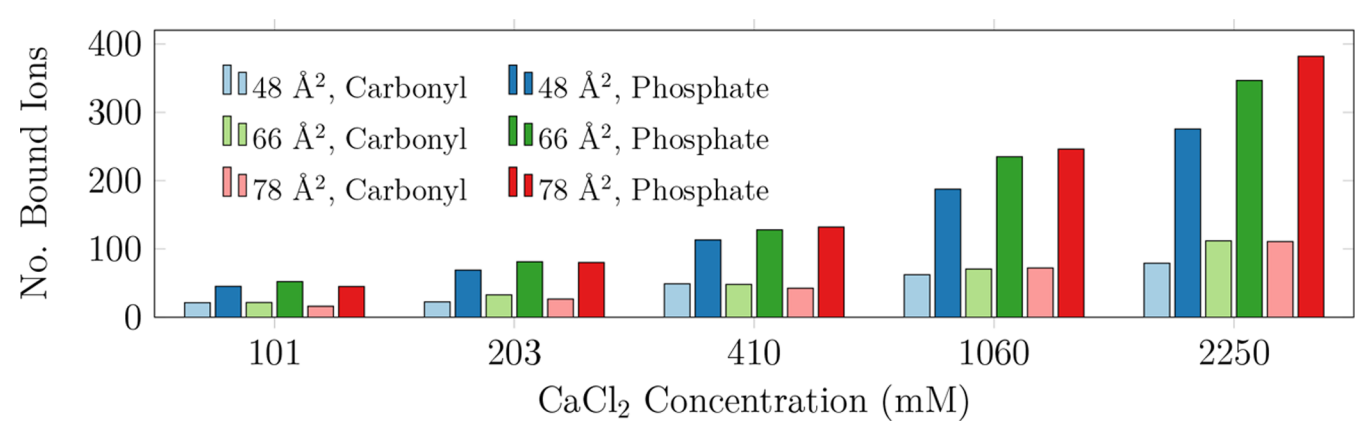


Figure 5. Binding preference of Ca^{2+} as a function of APL in $Å^2$ (coloring) and $CaCl_2$ concentration (x-axis). The binding is resolved between carbonyl and phosphate oxygens. Notably, as a single ion can simultaneously fulfill the criteria of binding into both types of oxygens, the total number of bound ions is smaller than the sum of the two bars.

binding to the carbonyl groups seems to be somewhat saturated and there is little difference between binding to these groups in the monolayers with the two largest APLs. However, at the high CaCl₂ concentrations, the phosphate oxygens bind a substantial amount of cations. As discussed earlier, this binding to phosphates seems to have little effect on lipid packing and hence on surface pressure (see Figure 4). The binding of Cl⁻ ions to lipids via Ca²⁺ bridges again showed the same shape and tendency as the Ca²⁺ binding (see bottom row in SI Figure S5). The Ca²⁺ adsorption to the monolayer also leads to the dehydration of lipid head groups, as demonstrated by SI Figure S7.

In addition to global effects manifested in phase behavior, lipid—ion interaction can also lead to conformational changes in the lipid headgroup. This is well described by the deuterium order parameters $S_{\rm CD}$ of the hydrocarbon segments of the lipid headgroup. ^{8,46} We calculated the deuterium order parameters for the two carbon atoms labeled in Figure 10 as a function of CaCl₂ concentration, and the results are shown in Figure 6.

Based on Figure 6, already a presence of a small amount of CaCl, has a significant effect on the headgroup conformation.

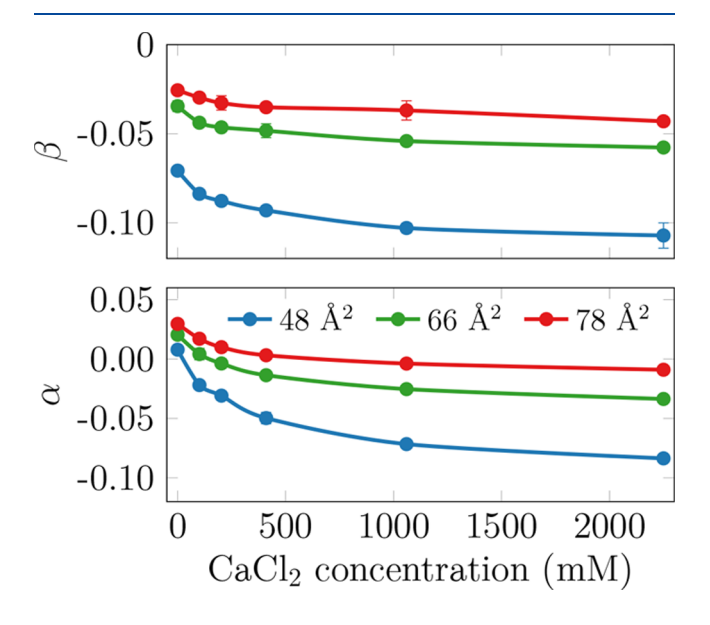


Figure 6. Dependency of lipid headgroup deuterium order parameters on CaCl₂ concentration.

While an increasing CaCl₂ concentration has an ever smaller effect on the order parameters, the change is still measurable and systematic. The shapes of the curves in Figure 6 agree with those measured for lipid bilayers in both experiments⁴⁶ and simulations with the ECC lipid model.¹¹ Curiously, the magnitude of the effect of CaCl₂ depends on monolayer packing; the smaller the monolayer APL, the more drastic the conformational changes seem to be. However, such comparison should be avoided as the dependence of the deuterium order parameter on lipid headgroup tilt is not linear.

To have a more detailed view on the effect of CaCl₂ concentration and APL on the headgroup conformations, we performed computer clustering analysis on the population of lipids aggregated from all performed simulations with varying CaCl₂ concentrations. An equal number of lipid molecules was randomly selected from each of the 18 simulations with varying area per lipid (48, 66, and 78 Å²) and the Ca²⁺ concentration (0, 101, 203, 410, 1060, and 2250 mM). According to their conformation the lipid molecules were separated into "clusters", considering only the positions of atoms, and treating all lipid molecules separately and equally (see Methods for details).

Since the clustering algorithm is ignorant about external conditions of the simulations (the APL and the CaCl₂ concentration), differences between the clusters can be attributed to effects of these conditions. In particular, the relative abundance of lipids from different simulations in individual clusters can be used to analyze the magnitude of the effect of the varying condition (APL or CaCl₂ concentration) on the lipid conformation and also a possible correlation between the effects.

Since the number of conformations is not known a priori, clustering analysis was performed for different number of clusters. The conformations are distributed continuously (homogeneously covering part of the physical space) signifying that the number of clusters can not be guessed from the clustering results. Conversely, different number of clusters can be used depending on the analysis specifics, a small number of clusters (12) was used for detailed analysis of each representative conformation while a large number (64) of clusters was used especially for visual analysis of the bulk properties.

Twelve different conformations can be readily distinguished in SI Figure S8. All such clusters are significant in terms of

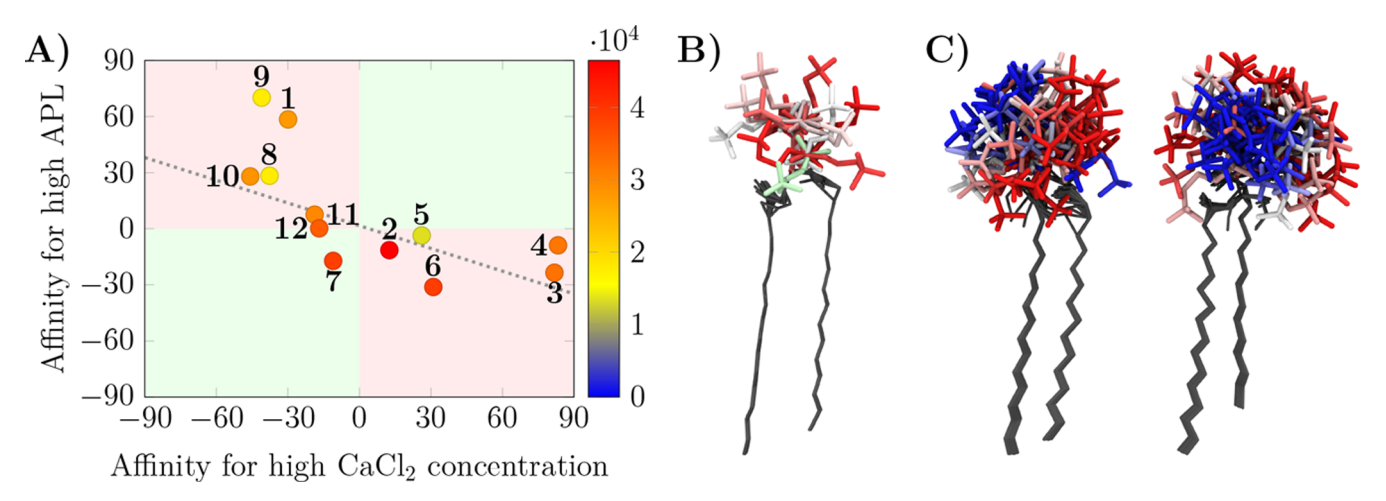


Figure 7. A) Correlation between the impacts of CaCl₂ concentration and APL on the lipid headgroup conformation. Numbered dots signify individual clusters, where the color symbolizes the total cluster abundance. A clear anticorrelation can be observed, the conformation No. 7 being the only outlier. Linear fit of the data weighted by the relative cluster abundance (dashed gray line) exhibits a slope of -0.4 and an offset of 1.6. The range of the affinity toward CaCl₂ concentration is slightly higher than for APL (-50 to +80 vs -30 to +70) signifying that the lipid conformation is affected more by the former. B) Representative conformations colored by the correlation of the cluster abundance between the CaCl₂ concentration and the APL within the respective cluster, (green: correlated, white: no correlation, red: anticorrelated), the shade specifies the total CaCl₂ concentration and APL dependence magnitude (light: low dependence, dark: high dependence). See 10.6084/m9.figshare.12783584 for additional visualization. C) The clusters—or the representative lipid conformations—can be classified by their affinity to concentrated Ca²⁺ environment. The measure of such affinity can be defined as a slope of the relative abundance as a function of concentration. Positive values (blue) signifies affinity to high CaCl₂ concentrations while negative (red) to low ones. See 10.6084/m9.figshare.12783584 for additional visualization.

abundance (SI Figure S9). The relative cluster abundances within each of the different simulations (cluster compositions) were analyzed statistically. If the composition of a cluster is not uniform with respect to the external condition (APL or CaCl₂ concentration) it is influenced—either directly or indirectly via a correlation—by that condition. All clusters (representative conformations) are indeed affected by the CaCl₂ concentration and most clusters also by the area per lipid (SI Figure S9).

The degree (magnitude) of influence can be defined as the derivative of the cluster abundance as a function of the external condition ξ . The value is normalized by the absolute abundance of individual clusters (in order to compare clusters of different sizes) and by the explored ranges of the conditions ξ (to enable comparison between the conditions). Positive values represent affinity toward a high condition ξ , while negative values represent affinity to a low ξ . The affinity can also be viewed as increased probability to find a lipid of selected conformation as the condition ξ increases. The average magnitude of the influence for each cluster was estimated through linear fitting.

The CaCl₂ concentration has a higher impact on distribution of the lipid population among the clusters than the area per lipid. A clear anticorrelation can be observed between the two in Figure 7A. In other words, if the relative abundance of a given conformation increases with CaCl₂ concentration, it decreases with APL and vice versa. The 12 representative conformations colored by the magnitude and the sign of the correlation can be seen in Figure 7B.

Next, we focused on the effect of CaCl₂ concentration on the cluster populations, as the effects of APL are mostly the opposite based on the anticorrelation in SI Figure S9. The degree of influence can be used to further separate the clusters into two groups: those with a positive or a negative affinity toward higher CaCl₂ concentrations. It turns out that the clusters are not randomly distributed among the groups, but rather the groups divide the physical conformation space into

two areas, hemispheres (Figure 7C). That means that the conformations with an affinity toward higher CaCl₂ concentrations are physically similar. It is also evident from Figure 7C that an increase in CaCl₂ concentration results in more compact packing of the headgroup.

To further clarify the effect of CaCl₂ on the individual lipid head groups, we performed vibrational sum frequency generation (VSFG) spectroscopy measurements of the phosphate group. As shown in Figure 8, two distinct peaks at ~1070 and ~1100 cm⁻¹ are observed in all the spectra and are assigned to the phosphate ester stretch near the choline moiety $(\nu(P-O-(C^{C})))^{-1}$ and the PO_{2}^{-1} symmetric stretch $(\nu_{s}(PO_{2}^{-1}))$, respectively.^{47,48} A very weak band on the low frequency side of the $\nu_s(PO_2^-)$ peak is observed at ~1090 cm⁻¹ and was suggested to be due to the R-O-P-O-R' stretch. 49 At constant Cl⁻ concentration, the intensity of the 1070 and 1100 cm⁻¹ peaks decrease to a different extent on salt solutions relative to water, with the peak intensity following the order of neat water $> Na^+ > Ca^{2+}$. In the low concentration regime, Ca^{2+} is the only cation that induces a blue shift (~4 cm⁻¹) of the $\nu_s(PO_2^-)$ peak, indicating a significant change in the hydration environment of the phosphate moiety, in line with simulations (see SI Figure S7). Moreover, in comparison to neat water, Ca2+ give rise to peak broadening (full width at half-maximum (fwhm) of ~26 to 32 cm⁻¹) of $\nu_s(PO_2^-)$, whereas Na⁺ ions cause minimal changes. The $\nu_s(PO_2^-)$ peak broadening likely arises from the structural heterogeneity of the hydrated phosphate. Cation effects on the phosphate groups at higher concentrations are demonstrated in Figure 8 as well. Similar to the results in the low concentration regime, an intensity decrease is seen for all the spectra with increasing salt concentration although more pronounced. No blue shift is observed for Na+ even at these higher concentrations, while a significantly larger blue shift of $\nu_s(PO_2^-)$ is induced by Ca^{2+} (~12 cm⁻¹). Only in the highly concentrated aqueous Ca²⁺ regime (>2 M), the emergence of a strong peak with a blue

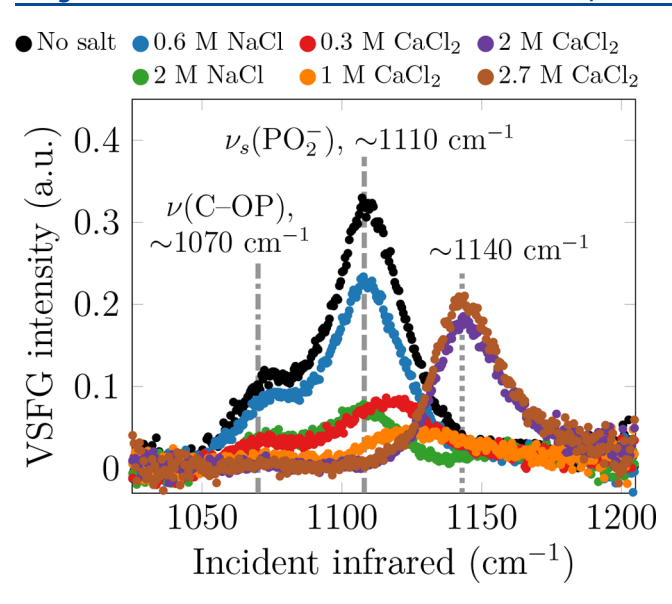


Figure 8. Vibrational sum frequency generation spectra (*SSP* polarization) of DPPC monolayers spread on CaCl₂ subphases revealing dramatic changes in intensity and frequency coinciding with increasing calcium chloride concentrations indicative of differing binding motifs. The dashed gray line highlights the alignment of the peaks measured in the absence of salt and with 600 mM of NaCl at $\sim 1108~\rm cm^{-1}$, whereas the dotted gray line shows the alignment of the peaks at $\sim 1143~\rm cm^{-1}$ measured for CaCl₂ concentrations of 2 and 2.7 M. The dash-dotted line highlights the peak at $\sim 1170~\rm cm^{-1}$.

shift of $\sim 35~{\rm cm}^{-1}$ concurrent with the disappearance of the phosphate symmetric stretch. The observed spectral blue shift is consistent with computational studies on dimethyl phosphate (DMP⁻) in the presence of Ca²⁺ that have shown that as the Ca²⁺ cation approaches the anionic oxygens, a blue shift of the PO₂⁻ symmetric mode is seen. ⁵⁰

To find a molecular explanation for the behavior of the VSFG spectra, we calculated the density profiles of Ca²⁺ and Cl⁻ ions together with the phosphorus atoms from simulations at 66 Å² and at different ion concentrations. Selected profiles are shown in the top three panels of Figure 9. Curiously, we find that the shift and saturation of the peak in the VSFG spectrum coincides with the penetration of Cl⁻ ions to the region below the phosphorus atoms of DPPC. The numbers of ions that penetrate below the phosphorus density peak are plotted in the bottom panel of Figure 9. At low concentrations, there are more Ca2+ ions in this region, yet the numbers are fairly small. However, after ~700 mM, there are more Cl⁻ than Ca²⁺ ions below the phosphorus level, and at the largest studied concentration Cl⁻ dominates by already ~45%. This effect is also visually evident in Figure 10, which shows a typical arrangement of ions at the surface of a monolayer with an APL of 66 Å² at 2.25 M of CaCl₂. The Ca²⁺ ions, shown in yellow, are bound to the phosphate group, whereas the Clions, shown in green, can penetrate to beyond this region and all the way to the vicinity of the carbonyl groups. Since the carbonyl oxygens bear a negative partial charge, this arrangement is likely stabilized by the overcharging at the phosphate level caused by the large amounts of Ca2+ ions therein.5

DISCUSSION AND CONCLUSIONS

In this work, we combined molecular dynamics simulations with Langmuir trough measurements and vibrational sum frequency generation spectroscopy to unravel the effect of

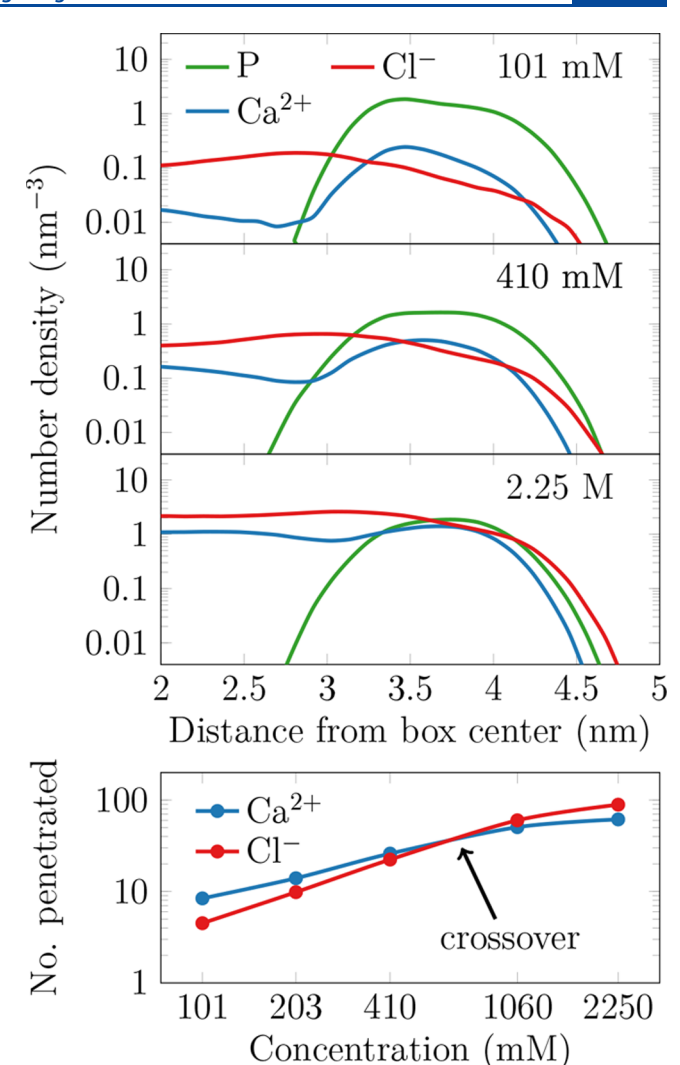


Figure 9. Top three panels: Number density profiles of phosphorus (P), calcium, and chloride on the monolayer surface at an APL of 66 \mathring{A}^2 as a function of CaCl₂ concentration for selected systems. Bottom panel: The number of ions that have penetrated below the phosphorus level, shown in the log–log scale. At ~700 mM, the number of penetrated Cl⁻ becomes larger than that of Ca²⁺.

cations on the properties of lipid monolayers. To this end, we have simulated DPPC monolayers at various compression states and in the presence of NaCl and CaCl₂. The force fields used for DPPC, water, and ions were all state-of-the-art and accurately describe the behavior of lipids at water—air interfaces²² as well as the lipid—ion interactions.¹¹ The simulated systems cover the liquid condensed and liquid expanded phases, and their coexistence. For CaCl₂, additional simulations where performed with multiple salt concentrations for three compression states that correspond to the two studied monolayer phases and their coexistence. Experimentally, we evaluated the effects of NaCl and CaCl₂ on Langmuir isotherms and studied the effect of various CaCl₂ concentrations on the vibrational spectrum of the phosphate group in the DPPC headgroup.

We first obtained surface pressure—area isotherms from both experiments and simulations. From these isotherms in Figure 2, it is evident that the shapes of the simulated and experimental isotherms are not identical. Nevertheless, the simulated isotherm reproduces the characteristic plateau of

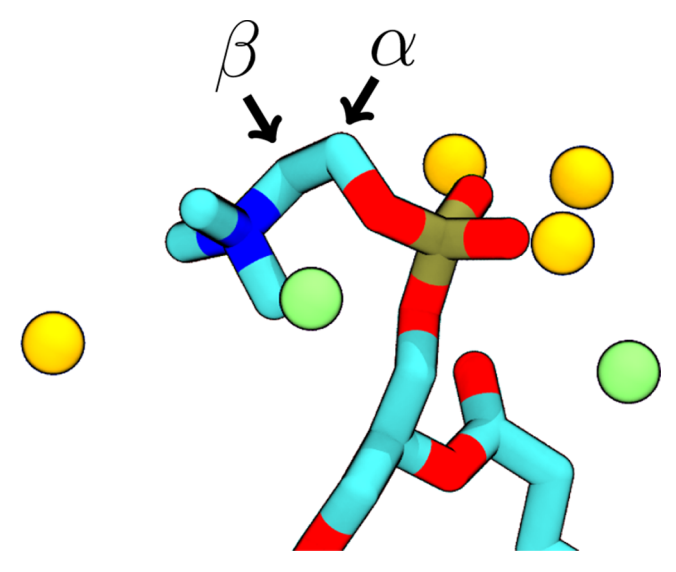


Figure 10. Characteristic conformation of the DPPC headgroup and bound ions under high CaCl₂ concentrations. Here, carbons are shown in cyan, oxygen in red, phosphorus in brown, and nitrogen in blue. Ca²⁺ and Cl⁻ ions are shown in yellow and green, respectively. Hydrogens and water are omitted for clarity. The labels indicate the carbons for which deuterium order parameters are reported in Figure 6.

DPPC isotherms²² and the surface pressure values are mostly reasonable without any shifting of the isotherms.¹⁶ Moreover, it seems that at small areas per lipid the current ECC-based model performs better than CHARMM36 in our earlier work,²² whereas at larger areas CHARMM36 is in better agreement with experiment. Strikingly, at APL equal to 54 Å², the surface pressure in the system with CaCl₂ reaches a negative value. It seems that at this area, CaCl₂ is able to cluster the lipids efficiently, which in a finite simulation box leads to a phase separation between tightly packed clusters and small amounts of exposed surface. Despite these limitations, the simulation model seems to capture well the effect of ions on the pressure—area isotherms and justifies our attempts to explain the experimentally observed behavior based on simulation data.

We then evaluated how monolayer packing and cation type affect the adsorption of ions to the monolayer surface. The dependence of cation—lipid contacts on APL (bottom panel in Figure 2) agrees well with our recent study⁶ despite the fact that no ECC lipids were used therein: Na⁺ binding depends only on the amount of PC head groups available for binding, whereas the adsorption of Ca²⁺ depends on the surface area available for binding. The saturation of Ca²⁺ binding at large areas (bottom panel in Figure 2) is a new observation, and likely results from the fact that the loosely packed lipid—water interface undergoes charge inversion. This is more likely with the ECC lipids used in this work (in contrast to ref 6), as the inversion happens at a smaller amount of bound Ca²⁺.

Both simulations and experiments demonstrated a condensing effect of $CaCl_2$ on the monolayers, whereas NaCl was not found to have an effect on lipid packing. The effect of $CaCl_2$ was most present in the L_c/L_c coexistence region, where the surface pressures were lowered by $CaCl_2$. The simulations revealed that this condensation resulted from an increase in the fraction of the L_c phase, whereas the properties of the individual phases were not affected. Simulations with varying

CaCl₂ concentrations demonstrated that the condensing effect of CaCl₂ is strong at relatively small concentrations and the effects saturate at ~400 mM. Still, a further increase in CaCl₂ concentration affected the conformations of lipid head groups (Figures 6 and 7). Our cluster analysis revealed that increases in CaCl₂ concentration and APL affect the cluster populations in an anticorrelated way. Moreover, we observed that the clusters that are more preferred at higher and lower CaCl₂ concentrations are physically distinct and populate two hemispheres. Moreover, higher CaCl₂ concentrations also prefer more compact headgroup conformations (Figure 7C). At concentrations above 2 M, the VSFG spectra (Figure 8) displayed drastic effects in the phosphate region. Unfortunately, due to its quantum-mechanical nature, a VSFG spectrum cannot be resolved from our atomistic simulations. Moreover, performing quantum-mechanical calculations for all the lipid-cation geometries observed in our simulations is out of the reach of current resources. Therefore, we connected the VSFG spectra to properties available in our simulations, namely ion densities and binding modes. This approach revealed (Figure 5) that at high CaCl2 concentrations the binding to the carbonyl groups is fairly limited, whereas more ions adsorbed to the phosphate region and this binding was coupled with Cl⁻ ions penetrating deep below the phosphate region (Figure 9). This arrangement with Cl⁻ ions allowing more Ca²⁺ to bind to the phosphate region appears only at high CaCl₂ concentrations. We believe that this specific organization of ions is the new binding mode that appears in the VSFG spectrum at high CaCl₂ concentrations.

Based on our results, the changes in lipid packing take place at fairly low $CaCl_2$ concentrations and especially in the L_c/L_e coexistence region. However, lipid headgroup conformations are systematically affected by an increasing $CaCl_2$ concentration at least until the largest simulated concentration of 2.25 M. Curiously, the headgroup conformations of the L_c phase monolayer are most affected by $CaCl_2$. Finally, very large $CaCl_2$ concentrations introduce a new and mutual binding mode for Ca^{2+} and Cl^- detected in VSFG spectroscopy and our density profiles. Thus, it seems that the local (conformation and ion binding mode of a single lipid) and global (lateral packing of lipids) effects are not connected in a straightforward manner.

One limitation of the ECC framework worth mentioning here is that it is in principle limited to studies on systems that are heterogeneous in their electronic response, that is, lack any interfaces at which the electronic contribution to the dielectric constant changes abruptly. This is obviously not true for the water-air interface, and different scaling factors should therefore be applied on the two sides of the interface, 1 for the air phase and 0.75 for the aqueous phase. 14 We are not aware of any simulation code which allows the definition of position-dependent ECC scaling factors or dielectric constants. Although it could be technically possible to estimate the electronic contribution to the dielectric constant across the water-lipid-air layers and scale the charges based on their location at each time step, this would be a major effort. Moreover, charge neutrality would potentially pose issues with such an approach. In this work, we notice that the use of the constant scaling factor of 0.75 leads to a too weak effect of salt on surface tension of the electrolyte solution, whereas the effect with unscaled charges is overestimated (see SI Figure S1 for the solvents used in this work, whereas a more complete figure is available in ref 14). Still, we consider this limitation

acceptable in terms of the present study, as the use of ECC ions remedies the more severe issue of ion—lipid overbinding. Other issues to be tackled in future work on ECC models—including the value of the charge scaling factor and the treatment of complex biomolecules with partial charges—are discussed in our recent review.¹⁴

Our results help us understand how ions can regulate local lipid packing in the DPPC-rich pulmonary surfactant monolayers, where the phase behavior of lipids is of key physiological importance. Namely, the balance of L_a and L_c phases is required for the proper folding of the pulmonary surfactant monolayer into lipid reservoirs during exhaling, as well as for the correct function of surfactant proteins.²⁵ However, application of our results to cellular membranes is likely less straightforward, as the behavior of monolayers used here depend heavily on their compression state. Still, the trends observed here especially for the headgroup conformations are likely similar despite the level of lipid packing. Still, cellular membranes are very complex entities with thousands of lipid components, proteins, and other molecules. Notably, they have other means to control lipid packing, the most wellknown one being sterol molecules such as cholesterol.⁵² It is also worth noting that while the concentrations used here for NaCl are close to those present in the extracellular fluid (145 mM), the used CaCl2 concentrations are drastically higher than those present therein (1-2 mM).⁵³ In the cytosol, CaCl₂ is much more scarce, and its concentration remains smaller than in the extracellular fluid even during signaling-related calcium spikes.⁵⁴ Therefore, the possible applications of the high Ca²⁺ concentrations used in this study likely lie in the field of engineering and in marine-derived atmospheric aerosol chemistry, rather than in biosciences.

ASSOCIATED CONTENT

Supporting Information

The Supporting Information is available free of charge at https://pubs.acs.org/doi/10.1021/acs.langmuir.0c02555.

Optimization of the ECC ions for OPC water. Computational results on the surface tension of the lipid-free interface, on the convergence of the ion adsorption, on the Ca²⁺ binding preference as a function of area per lipid, and additional results on the clustering of lipid headgroup structures (PDF)

AUTHOR INFORMATION

Corresponding Authors

Matti Javanainen — Institute of Organic Chemistry and Biochemistry of the Czech Academy of Sciences, 160 00 Prague 6, Czech Republic; ⊚ orcid.org/0000-0003-4858-364X; Email: matti.javanainen@gmail.com

Heather C. Allen – Department of Chemistry and Biochemistry, The Ohio State University, Columbus, Ohio 43210, United States; orcid.org/0000-0003-3120-6784; Email: allen@chemistry.ohio-state.edu

Authors

Wei Hua – Department of Chemistry and Biochemistry, The Ohio State University, Columbus, Ohio 43210, United States Ondrej Tichacek – Institute of Organic Chemistry and Biochemistry of the Czech Academy of Sciences, 160 00 Prague 6, Czech Republic; orcid.org/0000-0002-3676-8367

Pauline Delcroix — J. Heyrovsky Institute of Physical Chemistry of the Czech Academy of Sciences, 18223 Prague 8, Czech Republic; ⊚ orcid.org/0000-0002-5482-3905 Lukasz Cwiklik — J. Heyrovsky Institute of Physical Chemistry of the Czech Academy of Sciences, 18223 Prague 8, Czech Republic; ⊚ orcid.org/0000-0002-2083-8738

Complete contact information is available at: https://pubs.acs.org/10.1021/acs.langmuir.0c02555

Notes

The authors declare no competing financial interest.

ACKNOWLEDGMENTS

M.J. thanks CSC-IT Center for Science for computational resources and the Emil Aaltonen foundation for funding. M.J. and O.T. acknowledge computational resources supplied by the project "e-Infrastruktura CZ" (e-INFRA LM2018140) provided within the program Projects of Large Research, Development and Innovations Infrastructures. M.J. and L.C. acknowledge the support from the Czech Science Foundation (EXPRO Grant 19-26854X). W.H. acknowledges Mr. Zishuai Huang for his assistance in the preparation of sample solutions. H.C.A. and W.H. acknowledge the support from the U.S. National Science Foundation (NSF) grant CHE-1111762, and through the NSF Center for Aerosol Impacts on Chemistry on the Environment, grant CHE-1305427). O.T. acknowledges the Faculty of Mathematics and Physics of the Charles University (Prague, Czech Republic) where he is enrolled as a PhD student and the International Max Planck Research School for "Many-Particle Systems in Structured Environments" (Dresden, Germany) for support. P.D. acknowledges the support from the Czech Science Foundation (grant 17-06792S). We thank Dr. Samuli Ollila for constructive comments.

REFERENCES

- (1) Dodd, A. N.; Kudla, J.; Sanders, D. The Language of Calcium Signaling. *Annu. Rev. Plant Biol.* **2010**, *61*, 593–620.
- (2) Verdaguer, N.; Corbalan-Garcia, S.; Ochoa, W. F.; Fita, I.; Gómez-Fernández, J. C. Ca^{2+} Bridges the C2Membrane-Binding Domain of Protein Kinase $C\alpha$ Directly to Phosphatidylserine. *EMBO J.* **1999**, *18*, 6329–6338.
- (3) Bilkova, E.; Pleskot, R.; Rissanen, S.; Sun, S.; Czogalla, A.; Cwiklik, L.; Róg, T.; Vattulainen, I.; Cremer, P. S.; Jungwirth, P.; Coskun, U. Calcium Directly Regulates Phosphatidylinositol 4,5-Bisphosphate Headgroup Conformation and Recognition. *J. Am. Chem. Soc.* **2017**, *139*, 4019–4024.
- (4) Boettcher, J. M.; Davis-Harrison, R. L.; Clay, M. C.; Nieuwkoop, A. J.; Ohkubo, Y. Z.; Tajkhorshid, E.; Morrissey, J. H.; Rienstra, C. M. Atomic View of Calcium-Induced Clustering of Phosphatidylserine in Mixed Lipid Bilayers. *Biochemistry* **2011**, *50*, 2264–2273.
- (5) Sarmento, M. J.; Coutinho, A.; Fedorov, A.; Prieto, M.; Fernandes, F. Ca²⁺ Induces PI(4,5)P₂ Clusters on Lipid Bilayers at Physiological PI(4,5)P₂ and Ca²⁺ Concentrations. *Biochim. Biophys. Acta, Biomembr.* **2014**, 1838, 822–830.
- (6) Javanainen, M.; Melcrová, A.; Magarkar, A.; Jurkiewicz, P.; Hof, M.; Jungwirth, P.; Martinez-Seara, H. Two Cations, Two Mechanisms: Interactions of Sodium and Calcium With Zwitterionic Lipid Membranes. *Chem. Commun.* **2017**, *53*, 5380–5383.
- (7) Melcrová, A.; Pokorna, S.; Pullanchery, S.; Kohagen, M.; Jurkiewicz, P.; Hof, M.; Jungwirth, P.; Cremer, P. S.; Cwiklik, L. The Complex Nature of Calcium Cation Interactions With Phospholipid Bilayers. *Sci. Rep.* **2016**, *6*, 38035.
- (8) Catte, A.; Girych, M.; Javanainen, M.; Loison, C.; Melcr, J.; Miettinen, M.; Monticelli, L.; Määttä, J.; Oganesyan, V.; Ollila, O.;

- Tynkkynen, J.; Vilov, S. The Electrometer Concept and Binding of Cations to Phospholipid Bilayers. *Phys. Chem. Chem. Phys.* **2016**.
- (9) Böckmann, R. A.; Grubmüller, H. Multistep Binding of Divalent Cations to Phospholipid Bilayers: A Molecular Dynamics Study. *Angew. Chem., Int. Ed.* **2004**, 43, 1021–1024.
- (10) Ishiyama, T.; Shirai, S.; Okumura, T.; Morita, A. Molecular Dynamics Study of Structure and Vibrational Spectra at Zwitterionoic Lipid/Aqueous KCl, NaCl, and CaCl₂ Solution Interfaces. *J. Chem. Phys.* **2018**, *148*, 222801.
- (11) Melcr, J.; Martinez-Seara, H.; Nencini, R.; Kolafa, J.; Jungwirth, P.; Ollila, O. S. Accurate Binding of Sodium and Calcium to a POPC Bilayer by Effective Inclusion of Electronic Polarization. *J. Phys. Chem.* B 2018, 122, 4546–4557.
- (12) Melcr, J.; Piquemal, J.-P. Accurate Biomolecular Simulations Account for Electronic Polarization. *Frontiers in Molecular Biosciences* **2019**, *6*. DOI: 10.3389/fmolb.2019.00143
- (13) Han, K.; Venable, R. M.; Bryant, A.-M.; Legacy, C. J.; Shen, R.; Li, H.; Roux, B.; Gericke, A.; Pastor, R. W. Graph—Theoretic Analysis of Monomethyl Phosphate Clustering in Ionic Solutions. *J. Phys. Chem. B* **2018**, *122*, 1484—1494.
- (14) Duboué-Dijon, E.; Javanainen, M.; Delcroix, P.; Jungwirth, P.; Martinez-Seara, H. A Practical Guide to Biologically-Relevant Molecular Simulations With Charge Scaling for Electronic Polarization. J. Chem. Phys. 2020, 153, No. 050901.
- (15) Simons, K.; Vaz, W. L. Model Systems, Lipid Rafts, and Cell Membranes. *Annu. Rev. Biophys. Biomol. Struct.* **2004**, 33, 269–295.
- (16) Lamberg, A.; Ollila, O. S. Comment on "Structural Properties of POPC Monolayers Under Lateral Compression: Computer Simulations Analysis. *Langmuir* **2015**, *31*, 886–887.
- (17) Kohagen, M.; Mason, P. E.; Jungwirth, P. Accounting for Electronic Polarization Effects in Aqueous Sodium Chloride *via* Molecular Dynamics Aided by Neutron Scattering. *J. Phys. Chem. B* **2016**, 120, 1454–1460.
- (18) Martinek, T.; Duboué-Dijon, E.; Timr, Š.; Mason, P. E.; Baxová, K.; Fischer, H. E.; Schmidt, B.; Pluhařová, E.; Jungwirth, P. Calcium Ions in Aqueous Solutions: Accurate Force Field Description Aided by *ab initio* Molecular Dynamics and Neutron Scattering. *J. Chem. Phys.* **2018**, *148*, 222813.
- (19) Pluhařová, E.; Fischer, H. E.; Mason, P. E.; Jungwirth, P. Hydration of the Chloride Ion in Concentrated Aqueous Solutions Using Neutron Scattering and Molecular Dynamics. *Mol. Phys.* **2014**, *112*, 1230–1240.
- (20) Dickson, C. J.; Madej, B. D.; Skjevik, Å. A.; Betz, R. M.; Teigen, K.; Gould, I. R.; Walker, R. C. Lipid14: The Amber Lipid Force Field. *J. Chem. Theory Comput.* **2014**, *10*, 865–879.
- (21) Izadi, S.; Anandakrishnan, R.; Onufriev, A. V. Building Water Models: A Different Approach. *J. Phys. Chem. Lett.* **2014**, *5*, 3863–3871.
- (22) Javanainen, M.; Lamberg, A.; Cwiklik, L.; Vattulainen, I.; Ollila, O. S. Atomistic Model for Nearly Quantitative Simulations of Langmuir Monolayers. *Langmuir* **2018**, *34*, 2565–2572.
- (23) Liekkinen, J.; de Santos Moreno, B.; Paananen, R. O.; Vattulainen, I.; Monticelli, L.; de la Serna, J. B.; Javanainen, M. Understanding the Functional Properties of Lipid Heterogeneity in Pulmonary Surfactant Monolayers at the Atomistic Level. *Front. Cell Dev. Biol.* 2020, DOI: 10.3389/fcell.2020.581016
- (24) Olżyńska, A.; Zubek, M.; Roeselova, M.; Korchowiec, J.; Cwiklik, L. Mixed DPPC/POPC Monolayers: All-Atom Molecular Dynamics Simulations and Langmuir Monolayer Experiments. *Biochim. Biophys. Acta, Biomembr.* **2016**, *1858*, 3120–3130.
- (25) Pérez-Gil, J. Structure of Pulmonary Surfactant Membranes and Films: The Role of Proteins and Lipid—protein Interactions. *Biochim. Biophys. Acta, Biomembr.* **2008**, *1778*, 1676–1695.
- (26) Bruland, K.; Lohan, M. Controls of Trace Metals in Seawater. *Oceans and Marine Geochemistry* **2006**, *6*, 23–47.
- (27) Leontyev, I.; Stuchebrukhov, A. Accounting for Electronic Polarization in Non-Polarizable Force Fields. *Phys. Chem. Chem. Phys.* **2011**, *13*, 2613–2626.

- (28) Kirby, B. J.; Jungwirth, P. Charge Scaling Manifesto: A Way of Reconciling the Inherently Macroscopic and Microscopic Natures of Molecular Simulations. *J. Phys. Chem. Lett.* **2019**, *10*, 7531–7536.
- (29) Abraham, M. J.; Murtola, T.; Schulz, R.; Páll, S.; Smith, J. C.; Hess, B.; Lindahl, E. GROMACS: High Performance Molecular Simulations Through Multi-level Parallelism From Laptops to Supercomputers. *SoftwareX* **2015**, *1*, 19–25.
- (30) Essman, U.; Perera, L.; Berkowitz, M.; Darden, T.; Lee, H.; Pedersen, L. A Smooth Particle Mesh Ewald Potential. *J. Chem. Phys.* **1995**, *103*, 8577–8592.
- (31) Shirts, M. R.; Mobley, D. L.; Chodera, J. D.; Pande, V. S. Accurate and Efficient Corrections for Missing Dispersion Interactions in Molecular Simulations. *J. Phys. Chem. B* **2007**, *111*, 13052–13063.
- (32) Páll, S.; Hess, B. A Flexible Algorithm for Calculating Pair Interactions on SIMD Architectures. *Comput. Phys. Commun.* **2013**, 184, 2641–2650.
- (33) Bussi, G.; Donadio, D.; Parrinello, M. Canonical Sampling Through Velocity Rescaling. *J. Chem. Phys.* **2007**, *126*, No. 014101.
- (34) Hess, B.; Bekker, H.; Berendsen, H. J.; Fraaije, J. G. LINCS: A Linear Constraint Solver for Molecular Simulations. *J. Comput. Chem.* **1997**, *18*, 1463–1472.
- (35) Hess, B. P-LINCS: A Parallel Linear Constraint Solver for Molecular Simulation. *J. Chem. Theory Comput.* **2008**, *4*, 116–122.
- (36) Michaud-Agrawal, N.; Denning, E. J.; Woolf, T. B.; Beckstein, O. MDAnalysis: A Toolkit for the Analysis of Molecular Dynamics Simulations. *J. Comput. Chem.* **2011**, *32*, 2319–2327.
- (37) McAdams, A.; Selle, A.; Tamstorf, R.; Teran, J.; Sifakis, E. Computing the Singular Value Decomposition of 3 × 3 Matrices With Minimal Branching and Elementary Floating Point Operations, 2011.
- (38) Ollila, O. S.; Pabst, G. Atomistic Resolution Structure and Dynamics of Lipid Blayers in Simulations and Experiments. *Biochim. Biophys. Acta, Biomembr.* **2016**, *1858*, 2512–2528.
- (39) Humphrey, W.; Dalke, A.; Schulten, K. VMD Visual Molecular Dynamics. *J. Mol. Graphics* **1996**, *14*, 33–38.
- (40) Stone, J. An Efficient Library for Parallel Ray Tracing and Animation. M.Sc. thesis, Computer Science Department, University of Missouri-Rolla, 1998.
- (41) Hua, W.; Verreault, D.; Adams, E. M.; Huang, Z.; Allen, H. C. Impact of Salt Purity on Interfacial Water Organization Revealed by Conventional and Heterodyne-Detected Vibrational Sum Frequency Generation Spectroscopy. J. Phys. Chem. C 2013, 117, 19577–19585.
- (42) Finlayson, A. The pH range of the Mohr Titration for Chloride Ion Can Be Usefully Extended to 4–10.5. *J. Chem. Educ.* **1992**, *69*, 559.
- (43) Hua, W.; Verreault, D.; Huang, Z.; Adams, E. M.; Allen, H. C. Cation Effects on Interfacial Water Organization of Aqueous Chloride Solutions. I. Monovalent Cations: Li⁺, Na⁺, K⁺, and NH₄⁺. *J. Phys. Chem. B* **2014**, *118*, 8433–8440.
- (44) Adams, E. M.; Casper, C. B.; Allen, H. C. Effect of Cation Enrichment on Dipalmitoylphosphatidylcholine (DPPC) Monolayers at the Air–Water Interface. *J. Colloid Interface Sci.* **2016**, 478, 353–364.
- (45) Dean, J. A. Lange's Handbook of Chemistry; McGraw-Hill, Inc.: New York, 1999.
- (46) Akutsu, H.; Seelig, J. Interaction of Metal Ions With Phosphatidylcholine Bilayer Membranes. *Biochemistry* **1981**, 20, 7366–7373.
- (47) Casal, H. L.; Mantsch, H. H. Polymorphic Phase Behaviour of Phospholipid Membranes Studied by Infrared Spectroscopy. *Biochim. Biophys. Acta, Rev. Biomembr.* **1984**, *779*, 381–401.
- (48) Hübner, W.; Mantsch, H. H. Orientation of Specifically ¹³C = O Labeled Phosphatidylcholine Multilayers From Polarized Attenuated Total Reflection FT-IR Spectroscopy. *Biophys. J.* **1991**, *59*, 1261–1272.
- (49) Arrondo, J.; Goni, F.; Macarulla, J. Infrared Spectroscopy of Phosphatidylcholines in Aqueous Suspension a Study of the Phosphate Group Vibrations. *Biochim. Biophys. Acta, Lipids Lipid Metab.* 1984, 794, 165–168.

- (50) Petrov, A. S.; Funseth-Smotzer, J.; Pack, G. R. Computational Study of Dimethyl Phosphate Anion and its Complexes With Water, Magnesium, and Calcium. *Int. J. Quantum Chem.* **2005**, *102*, 645–655.
- (51) Hua, W.; Verreault, D.; Allen, H. C. Solvation of Calcium—Phosphate Headgroup Complexes at the DPPC/Aqueous Interface. *ChemPhysChem* **2015**, *16*, 3910—3915.
- (52) Róg, T.; Pasenkiewicz-Gierula, M.; Vattulainen, I.; Karttunen, M. Ordering Effects of Cholesterol and Its Analogues. *Biochim. Biophys. Acta, Biomembr.* **2009**, *1788*, 97–121.
- (53) Alberts, B.; Bray, D.; Hopkin, K.; Johnson, A. D.; Lewis, J.; Raff, M.; Roberts, K.; Walter, P. *Essential Cell Biology*; Garland Science, 2013.
- (54) Ross, W. N. Understanding Calcium Waves and Sparks in Central Neurons. *Nat. Rev. Neurosci.* **2012**, *13*, 157.